International Journal of Thermophysics, Vol. 27, No. 2, March 2006 (© 2006)
DOI: 10.1007/s10765-005-0001-6

Thermophysical Properties of Solid and Liquid Ti-6Al-4V (TA6V) Alloy

M. Boivineau,[1,2] C. Cagran,[3] D. Doytier,[1] V. Eyraud,[1] M.-H. Nadal,[1] B. Wilthan,[3] and G. Pottlacher[3]

Received May 24, 2005

Ti-6Al-4V (TA6V) titanium alloy is widely used in industrial applications such as aeronautic and aerospace due to its good mechanical properties at high temperatures. Experiments on two different resistive pulse heating devices (CEA Valduc and TU-Graz) have been carried out in order to study thermophysical properties (such as electrical resistivity, volume expansion, heat of fusion, heat capacity, normal spectral emissivity, thermal diffusivity, and thermal conductivity) of both solid and liquid Ti-6Al-4V. Fast time-resolved measurements of current, voltage, and surface radiation and shadowgraphs of the volume have been undertaken. At TU-Graz, a fast laser polarimeter has been used for determining the emissivity of liquid Ti-6Al-4V at 684.5 nm and a differential scanning calorimeter (DSC) for measuring the heat capacity of solid Ti-6Al-4V. This study deals with the specific behavior of the different solid phase transitions (effect of heating rate) and the melting region, and emphasizes the liquid state ($T > 2000$ K).

KEY WORDS: emissivity; phase transitions; Ti-6Al-4V; thermal conductivity; thermophysical properties; titanium alloys.

1. INTRODUCTION

During the last three decades, dynamic resistive heating techniques have been widely used for investigating the thermophysical properties of solid and particularly liquid metals in the temperature range $T > 1500$ K [1]. The

[1] Commissariat à l'Energie Atomique, Centre de Valduc, Département de Recherche sur les Matériaux Nucléaires, 21120 Is-sur-Tille, France.
[2] To whom correspondence should be addressed. E-mail: michel.boivineau@cea.fr
[3] Institut für Experimentalphysik, Technische Universität Graz, Petersgasse 16, A-8010 Graz, Austria.

main reason is that conventional heating techniques are not suited to the study of liquid metals due to their high chemical reactivity caused by contamination and exothermic reactions from the crucibles.

However, most of the studies have been devoted to nearly pure metals, of which a summary is given in the review papers of Gathers [2] or Cezairliyan [3]. During the last decade, a few laboratories have dealt with the study of liquid metallic alloys, with attention on industrial metals such as Inconel 718, Ti-6Al-4V, and CF8M stainless steel [4, 5], 53Nb-47Ti (mass%) [6, 7], Ti-44Al-8Nb-1B [8], Fe-Al alloys [9], Fe-Ni alloys [10], Ni- or Co-based alloys [11], or We-Re refractory alloys [12]. Indeed, accurate thermophysical property measurements of liquid industrial alloys are required for high-temperature technologies [13, 14] (i) to improve the modeling of industrially relevant solidification processes in casting and welding, (ii) to understand, simulate, design, and improve new processing equipment, (iii) for obtaining phase diagrams, (iv) for obtaining temperature reference points, (v) for accurate assessment of potential accidents in the design of safe nuclear reactors, (vi) for basic theory such as critical points of metals determination, which require high-temperature and high-pressure conditions, and (vii) for aerospace techniques (e.g., construction of low-pressure turbines blades, turbocharger rotors, etc).

The TiAl intermetallic alloy family has been widely used in this last domain because of its high mechanical properties (high strength/density ratio), such as stiffness, yield, fatigue, and creep strength, its principal weaknesses being its limited ductility and toughness at room temperature. Among the TiAl alloys, the Ti-6Al-4V (TA6V) alloy is considered as a standard material. As a result, such an alloy has been widely studied, but essentially in the solid state. Among the numerous studies reported in the literature regarding the solid, only a few have been reported up to the melting region [4, 15]. Moreover, to our knowledge, only one original study has been devoted to liquid Ti-6Al-4V [5] by reporting specific heat capacity and electrical resistivity measurements up to 2300 K. The purpose of the present study is thus an extension of the temperature range of the liquid phase.

2. GENERAL CONSIDERATIONS FOR THE TI-6AL-4V ALLOY

2.1. Ti-6Al-4V Phase Diagram

When alloying titanium, the additional elements mainly lead to the $\alpha + \beta$ solid solutions (with a large proportion of the α phase), such as Ti-6Al-4V. Inside this region and for a defined composition, the α phase proportion under equilibrium increases when the temperature decreases.

Moreover, such a region is separated from the β one-phase field whose transformation temperature T_β, the so-called β-transus, changes as a function of chemical composition. In the case of Ti-6Al-4V, the two additional elements, Al and V, result in opposite behaviors.

- Al (as for O, C, and N) is an active α -stabilizer (so-called alphagen element) and tends to increase T_β. The addition of such an element is correlated with hardening of the α phase, an increase of resistance, a decrease of ductility, and better resistance to extrusion.
- V (as for H, Mo, Ta, and Nb) is a typical β-stabilizer (so-called betagen element) and tends to decrease T_β. On the other hand, it increases the alloy resistance and is correlated with a decrease of resistance to oxidation (opposite to Mo).

Regarding the crystalline structures, it should be noted that the α phase is pseudo-hexagonal close-packed whereas β is body-centered cubic.

Figure 1 presents a partial phase diagram of the Ti-6Al alloy as a function of vanadium composition (up to 16% mass fraction) extracted from Ref. 16. This diagram indicates that the 4% V mass fraction line (corresponding to the Ti-6Al-4V alloy) intersects the β-transus temperature T_β at about 1280 K.

Moreover, melting ranges from 1873 to 1923 K (Goodfellow Cambridge Ltd. data). The values of most thermophysical properties are given in Ref. 17, and were used for welding applications. Since Al and V are lighter atoms than Ti, the alloy density (4.42) is lower than that for pure Ti (4.507) [17].

2.2. Chemical and Microstructure Analyses

Rod-shaped Ti-6Al-4V samples were provided by Goodfellow Ltd. The typical chemical analysis of Ti-6Al-4V samples is given in Table I according to the ASTMD 348-99 standard [18] referenced by Goodfellow Ltd.

Figure 2 presents the microstructure obtained from one single experiment where the sample is heated in the solid phase up to the β-phase by adjusting the current intensity. The micrographs are obtained at the frontier of the sample holder (no heating—cold zone) and the specimen (heated zone). As shown in Fig. 2, one can clearly distinguish both $\alpha + \beta$ (cold zone) and β (heated zone) phases. $\alpha + \beta$ presents an equiaxis-like structure with very fine grains (containing only a small proportion of the β phase). Unfortunately, little information is given from the

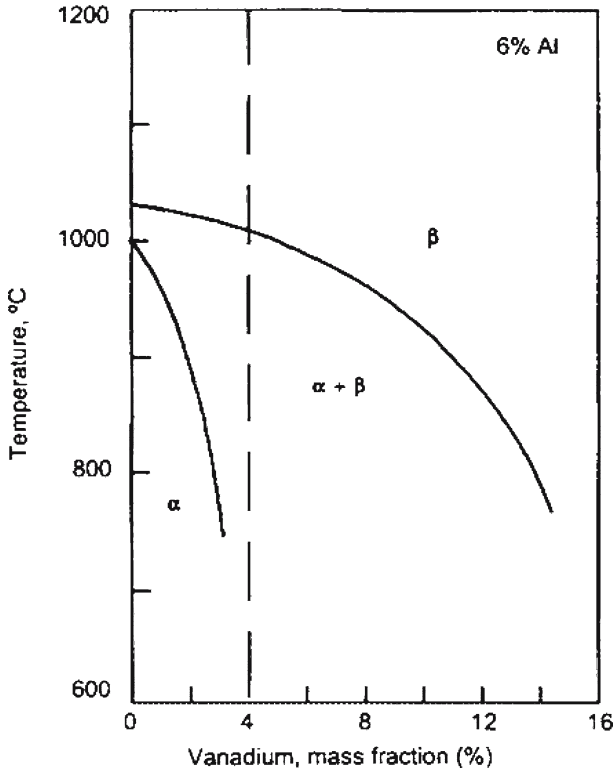

Fig. 1. Partial ternary phase diagram of Ti-6Al-V extracted from (Brooks, 1982) [16].

supplier regarding the manufacturing process. It seems to be typical for a cold-drawn microstructure obtained from an $\alpha + \beta$ structure. Moreover, the heated zone presents a β monophased needle-like microstructure with lamella of the α phase which is typical of a so-called Widmanstätten structure [19].

Table I. Typical Chemical Analysis of Ti-6Al-4V Alloys (ASTMD 348-99 Reference)

Element	Al	C	Fe	H	N	O	V	Ti
Composition (mass%)	6	0.1	0.4	0.015	0.05	0.2	3.5–4.5	Balance

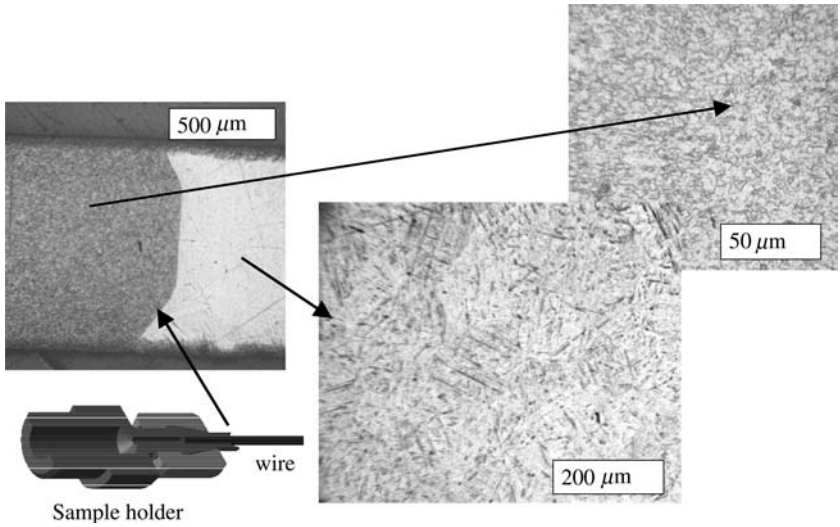

Fig. 2. Micrographs revealing microstructure differences of the $\alpha + \beta$ phase (not heated zone: top micrograph) and the β phase (heated zone: micrograph below).

3. GENERAL CONSIDERATIONS ON BOTH PULSE HEATING EXPERIMENTAL DEVICES

Both devices consist of rapid resistive self-heating of an electrical conducting specimen (typically a rod of a few hundred microns to a few millimeters diameter and a few centimeters in length) and heating them by the Joule effect. In other words, these experiments utilize the passage of a large electrical current pulse through the sample by discharging a capacitor bank with an appropriate time resolution of less than 1 s (typically from a few hundred milliseconds to a few hundred nanoseconds).

Among the numerous advantages of these dynamic techniques (number of accessible thermophysical data, exploration of the entire liquid state, determination of critical points, etc.), such methods are particularly relevant since the applied energy is imparted uniformly to the entire volume of the specimen (volume heating) in less than one second on the one hand, and permits the time dependence of some physical phenomena on the other hand.

Such dynamic methods can be classified according to various heating durations of the experiment and/or heating rates. Both devices belong to *microsecond resolution systems* and have been described in detail previously: Refs. 20 and 21 for CEA Valduc and Refs. 10 and 22 for TU-Graz, the heating duration being around 100 and 40 μs, respectively. Such

submillisecond devices have been developed for investigating thermophysical properties of materials in the temperature range of 2,000 to 10,000 K. The corresponding heating rate ranges from 10^6 to $10^8\,\mathrm{K}\cdot\mathrm{s}^{-1}$.

3.1. Measured and Calculated Quantities

At any instance, the following basic measurements are generally available: (i) current intensity through the sample $I(t)$; (ii) voltage drop along the sample $U(t)$; (iii) diameter of the sample $\phi(t)$; and (iv) thermal emission from the heated sample surface $J(t)$. Figure 3 presents such data for typical measurements on Ti-6Al-4V. These basic measurements already show the $\alpha+\beta-\beta$ solid transition from electrical measurements and melting throughout the pyrometer response.

From these measured quantities mentioned above, thermophysical properties, namely, enthalpy $H(t)$, electrical resistivity $\rho_{el}(t)$, specific volume $V/V_0(t)$ (and consequently density), thermal conductivity λ_T, thermal

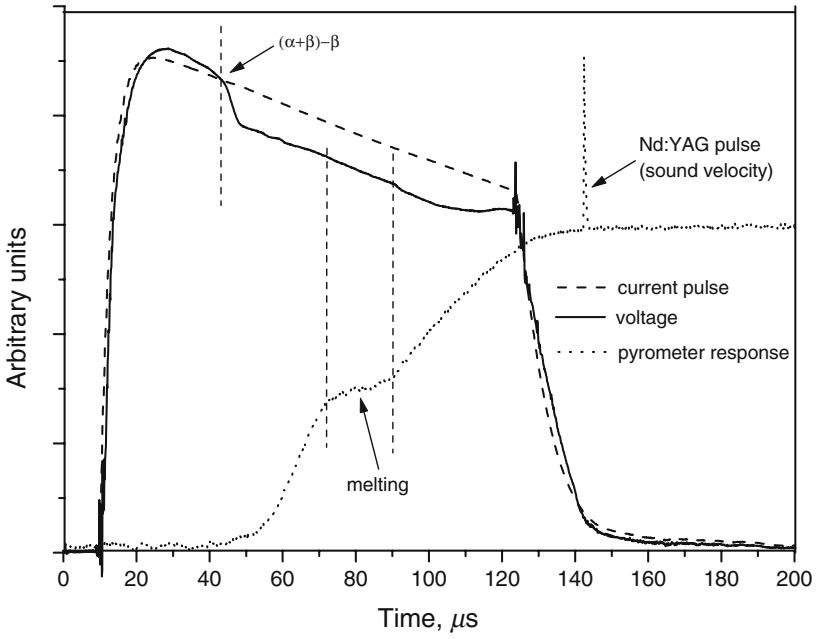

Fig. 3. Basic measurements (current intensity, voltage, pyrometer response) of a dynamic experiment performed on a Ti-6Al-4V specimen. The capacitor bank voltage is 7 kV producing a 6 kA current during 120 μs (CEA Valduc device). Sample dimensions are: 1 mm diameter, 30 mm length.

diffusivity a, and temperature $T(t)$ are calculated. By combining these different terms (which are all reported as a function of time), one obtains $H(T), \rho_{el0}(T), \rho_{el0}(H), \rho_{el}(T), \rho_{el}(H), V/V_0(T), V/V_0(H), a(T), \lambda_T$ (I) and the isobaric heat capacity c_p.

The enthalpy variation, equal to the internal (electrical) energy is then expressed by

$$\Delta H = H(T) - H(298) = \frac{1}{m} \int_{t_0}^{t} I(t) U_c(t) dt, \tag{1}$$

where m is the mass of the sample and U_c is the voltage corrected for the inductive term:

$$U_c(t) = U(t) - L \frac{dI(t)}{dt}, \tag{2}$$

where L is the self-inductance of the circuit.

It should be noted that due to the high heating rate (up to $10^8\ \mathrm{K} \cdot \mathrm{s}^{-1}$), radiative heat losses are assumed to be negligible. Such a consideration would not be true, for instance, for the millisecond systems (about $10^3\ \mathrm{K} \cdot \mathrm{s}^{-1}$).

The electrical resistivity is simply calculated from Ohm's law:

$$\rho_{el\,0}(t) = \frac{U_c(t)}{I(t)} \frac{\pi \phi_0^2}{4l}, \tag{3}$$

where ϕ_0 is the initial wire diameter and l is the distance associated with the potential difference measurement.

In most cases and when available, the radial expansion, and consequently the volume variation, is obtained by employing a shadowgraph technique with the use of a streak camera or a high frame rate CCD camera. Then a CW laser (or lamp) backlights the sample, whose shadow is viewed by the camera. Since supporting jaws block both ends of the wire, only radial expansion occurs.

A typical streak image is shown in Fig. 4. Consequently, image processing is used to obtain the relative radial expansion variation ϕ_t/ϕ_0. Since the sample maintains its cylindrical geometry throughout the solid and liquid states (before collapsing after the end of the experiment due to gravity or to phase explosion), and therefore the specific volume can be calculated from the following expression:

$$\frac{V(t)}{V_0} = \frac{\phi_t^2}{\phi_0^2}. \tag{4}$$

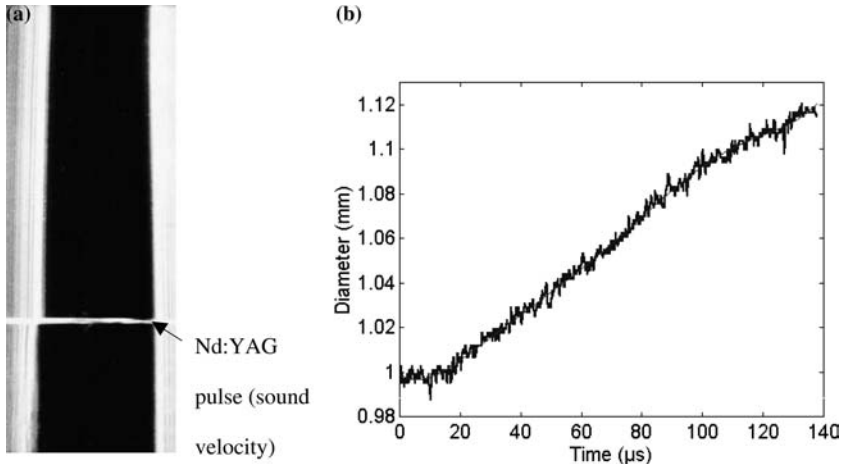

Fig. 4. (a) Radial expansion streak image of a wire-shaped Ti-6Al-4V sample and (b) correlated diameter variation as a function of time.

The density d (or specific gravity) can be calculated by using the mass conservation law as follows:

$$d = d_0 \frac{V_0}{V(t)} \tag{5}$$

where d_0 is the initial density of the sample.

The correct electrical resistivity ρ_{el} must take into account the radial expansion of the wire during heating. Then Eq. (3) becomes:

$$\rho_{el}(t) = \frac{U_c(t)}{I(t)} \frac{\pi \phi_t^2}{4l} = \rho_{el0}(t) \frac{\phi_t^2}{\phi_0^2}. \tag{6}$$

By knowing both the enthalpy (see Eq. (1)) and temperature (see Section 3.2), the specific heat capacity at constant pressure is also deduced from the following equation:

$$c_p = \left[\frac{\partial H(T)}{\partial T} \right]_{p=\text{const}}. \tag{7}$$

Some other thermophysical properties such as thermal conductivity and thermal diffusity can be determined. Indeed, the thermal conductivity λ_T is simply related to the electrical resistivity ρ_{el} from the Wiedemann–Franz law:

$$\lambda_T(T) = \frac{LT}{\rho_{el}(T)}, \tag{8}$$

where L is a constant, the so-called Lorentz number, i.e., $L = 2.45 \times 10^{-8}\,\mathrm{V}^2 \cdot \mathrm{K}^{-2}$. Equation (8) signifies the dominance of electrons in the heat transport and is known to work well for pure liquid metals [23].

The thermal diffusity may also easily be expressed from thermal conductivity according to

$$a(T) = \frac{\lambda_T(T)}{C_p(T) d_0}, \tag{9}$$

where d_0 is the initial density at room temperature.

3.2. Temperature Measurements

The TU-Graz system has recently integrated a new laser polarimeter permitting the determination of normal spectral emissivity. Such a tool is very relevant since the application of simultaneous laser polarimetry and spectral radiometry leads to a true temperature determination. Great advances have thus been achieved in temperature measurements by significantly improving their accuracy with such a device for a series of selected pure metals [24–26].

Briefly, it consists of the so-called microsecond-division of amplitude photopolarimeter (μs-DOAP) presented in Fig. 5. The physical basis of the μs-DOAP is to reflect an initially polarized laser beam (wavelength $\lambda = 684.5\,\mathrm{nm}$) from the pulse-heated liquid wire and to analyze the change

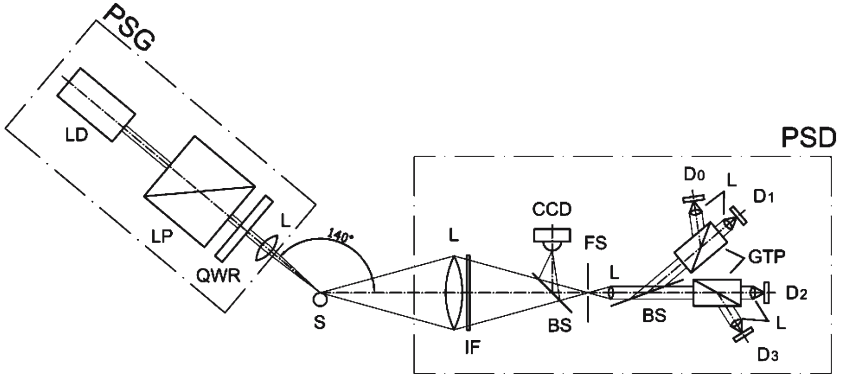

Fig. 5. Schematic setup of the μs-DOAP. PSD—polarization state generator with the following parts: LD—diode laser, LP—linear polarizer, QWR—quarter wave retarder, L—lens; S—sample; PSD: polarization state detector with the following parts: IF—interference filter, BS—beam splitter, CCD—CCD-camera, FS—field stop, GTP—Glan–Thompson-prism, D_0–D_3—detectors.

in polarization of the light upon reflection from the wire. Obtained properties are primarily the changes in optical constants n (refractive index) and k (extinction coefficient). Starting with these two optical constants, the normal spectral emissivity at 684.5 nm and its change during the experiment can be calculated.

Once n and k have been determined, the normal spectral reflectivity, R_λ, is calculated from the following equation:

$$R_\lambda = \frac{(n-n_0)^2+k^2}{(n+n_0)^2+k^2}, \tag{10}$$

where n_0 is the index of refraction of ambient gas ($n_0 \approx 1$ for air).

For opaque materials the normal spectral emissivity ε_λ is then determined from Kirchoff's law:

$$\varepsilon_\lambda = 1 - R_\lambda \tag{11}$$

From Eq. (11) and the determination of the sample *radiance* temperature T_R at a given wavelength, the true temperature T can be deduced from Wien's law:

$$\frac{1}{T} - \frac{1}{T_R} = \frac{\lambda}{c_2} \log \varepsilon_\lambda, \tag{12}$$

where λ is the wavelength, ε_λ is the normal spectral emissivity at the wavelength λ, and c_2 is the second Planck's constant (14388 μm · K).

3.3. Uncertainties

According to the guide to the expression of uncertainty in measurements [27], uncertainties reported here are expanded relative uncertainties with a coverage factor of $k = 2$. An evaluated set of uncertainties is given; for the measured pulse-heating data the following uncertainties are estimated: current, I, 2%; voltage drop, U, 2%; temperature, T, 4%; normal spectral emissivity, ε, 8%; mass m, 2%, from which we obtain for enthalpy, H, 4%; enthalpy of melting ΔH, 8%; specific heat capacity c_p, 8%, specific electrical resistivity with initial geometry, $\rho_{el,0}$, 4%, and specific electrical resistivity with volume expansion considered, ρ_{el}, 6%.

The estimated uncertainties of the thermal conductivity and thermal diffusivity are found to be 15% [10].

4. DSC MEASUREMENTS

To complete pulse heating data in the *solid* state, TU-Graz has also used a differential scanning calorimeter (DSC) which is described in Ref. 28. The specific heat capacity can be determined from room temperature up to 1500 K. The associated heating rates are typically $20\,\mathrm{K}\cdot\mathrm{min}^{-1}$, and this technique can be considered as a quasi-static process. Hence, by combining DSC and pulse-heating techniques, the complete temperature range of solid and liquid phases is investigated.

The DSC can be used primarily for measurements of the heat capacity of the sample (5.2 mm diameter and 0.5 mm height) in the temperature range from 500 to 1500 K. The sample is measured relative to a second, inert sample of approximately the same heat capacity. One experiment consists usually of three separate runs: a scan with two empty pans, a scan with one pan containing a sapphire reference sample, and finally a scan with the sample in the same pan where the reference sample was previously. The heat capacity as a function of temperature of the sample under investigation, $c_p(T)$, is obtained by using the following equation:

$$c_p(T) = c_p^{\mathrm{r}}(T)\frac{m^{\mathrm{r}}}{m}\frac{\Delta_3 - \Delta_1}{\Delta_2 - \Delta_1}, \tag{13}$$

where Δ_1, Δ_2, and Δ_3 are, respectively, the three DSC signals with empty pans, the signal of the reference, and the signal of the sample. m^r and m are the masses of the reference and the sample, respectively, and c_p^r is the heat capacity of the reference.

Using this heat capacity $c_p(T)$ obtained with DSC measurements, one is able to calculate the enthalpy of the specimen by integrating the heat capacity signal with respect to temperature and considering a constant c_p from room temperature to the start temperature of the experiment,

$$H_{298}(T) = \int_{473}^{T} c_p(T)\,dT + (473 - 298)c_p(473), \tag{14}$$

where $H(T)$ is the enthalpy and c_p is the specific heat capacity.

The assumption in Eq. (14) of a constant heat capacity between 298 and 473 K is taken into consideration for the uncertainty of the enthalpy values.

Therefore, the enthalpy versus temperature dependence for a given material can be calculated directly from DSC measurements. This enthalpy-temperature dependence can further be used to obtain the inverse

dependence, temperature versus enthalpy. With this result, one is able to extend our electrical measurements (i.e., enthalpy or electrical resistivity) of the pulse-heating experiments to lower temperatures by combining the temperature scale from the DSC (temperature versus enthalpy) with the electrical measured properties versus enthalpy. It has to be noted that the above mentioned procedure is only applicable as long as there are no phase transitions in the solid state of the material under investigation. Phase transitions can easily be observed with DSC measurements, but can be wholly or partially suppressed under pulse-heating conditions as applied within this experiment, due to the extreme high heating rates of $10^8\,\mathrm{K}\cdot\mathrm{s}^{-1}$. This procedure enables us to extend the results for enthalpy versus temperature and resistivity versus temperature to lower temperature regions, starting now at the onset temperature of the DSC (500 K). Up to now access to these temperature regions when using pulse-heating techniques was only possible by experiments with millisecond time resolution [29]. For the DSC data the uncertainties are: temperature, T, 2 K; specific heat capacity, c_p, 3%. The uncertainties of the temperature values after the merging of pulse-heating and DSC data results are dominated by the uncertainty of the enthalpy values obtained by pulse heating. Out of this, the uncertainty over the whole temperature interval is estimated to be 4%.

5. RESULTS AND DISCUSSION

5.1. Solid Phase

Figure 6 presents electrical resistivity measurements (not volume corrected) as a function of enthalpy for solid Ti-6Al-4V for the present work (microsecond systems) compared to literature data [5]. In all cases, it clearly shows the $(\alpha+\beta)-\beta$ transition by a strong electrical resistivity variation. Moreover, very good agreement between all the experiments is observed except for the millisecond experiment presenting a lower enthalpy value for the transition. Indeed, the β-transus strongly depends on the heating rate as first shown by Kaschnitz et al. [5] by using both millisecond (corresponding to a $10^3\,\mathrm{K}\cdot\mathrm{s}^{-1}$ heating rate) and microsecond ($10^7\,\mathrm{K}\cdot\mathrm{s}^{-1}$) systems. Present data are obtained with 5 and 7 kV CEA bank voltages corresponding to 1.3×10^7 and $2.3\times10^7\,\mathrm{K}\cdot\mathrm{s}^{-1}$ heating rates, respectively. In all cases, the β-transus is shifted towards larger enthalpy values and thus higher temperatures compared to the millisecond experiment. Such a phenomenon could be attributed to nonequilibrium conditions by using high heating rates and is probably enhanced for alloys compared to pure metals.

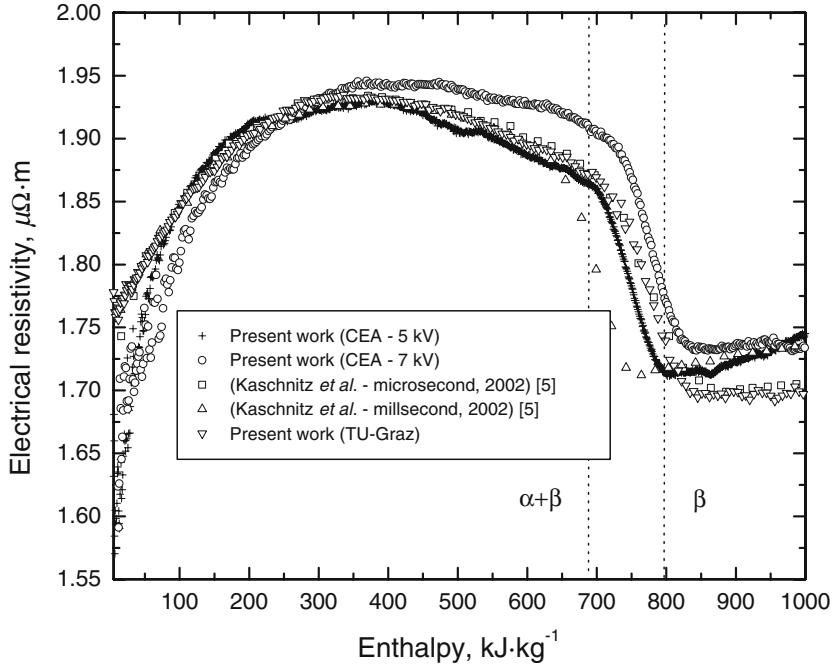

Fig. 6. Electrical resistivity as a function of enthalpy. The β-transus strongly depends on the heating rate as first shown by Kaschnitz et al. (2002) [5] by using both millisecond (corresponding to a $10^3\,\mathrm{K}\cdot\mathrm{s}^{-1}$ heating rate) and microsecond ($10^7\,\mathrm{K}\cdot\mathrm{s}^{-1}$) systems. Present data are obtained with 5 and 7 kV CEA bank voltages, and 6 kV TUG bank voltage corresponding to 1.3×10^7, 2.3×10^7, and $2.5\times10^7\,\mathrm{K}\cdot\mathrm{s}^{-1}$ heating rates, respectively.

The specific heat capacity at constant pressure C_p has also been studied by using the differential scanning calorimeter (TU-Graz) operating at continuous heating. Its variation versus temperature up to 1400 K is reported in Fig. 7. The peak observed at 1220 K corresponds to the β-transus line. It seems to be quite narrower than the one obtained by Basak et al. [4] from pulse-heating experiments. Such a difference is not well explained, but the specific heat capacity and electrical resistivity are known to strongly depend on the thermal history of the material. Moreover, the material behavior could be influenced by continuous (DSC) and pulse heating regimes (effect of heating rate).

It should be noted that variations of c_p are also observed from DSC experiments. Such reproducible variations occur at around 800 and 900 K and would correspond to endothermic and exothermic phenomena, respectively.

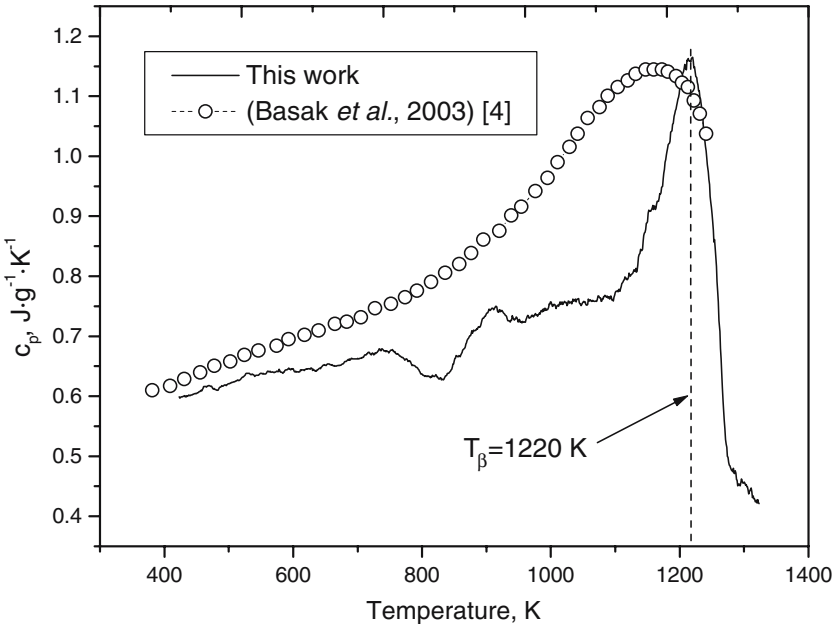

Fig. 7. Specific heat capacity of solid Ti-6Al-4V compared to literature data (Basak et al., 2003) [4].

5.2. Liquid State

Even with a high melting point, liquid Ti-6Al-4V has also been investigated. Figure 8 presents the electrical resistivity as a function of enthalpy in both solid and liquid states. Strong variations or change of slope are associated with phase transitions. Therefore, the β-transus and melting are clearly evidenced. From DSC measurements, the $(\alpha+\beta)-\beta$ transition was found to be at 1220 K (Fig. 7) which corresponds to an enthalpy value of $678\,\mathrm{kJ}\cdot\mathrm{kg}^{-1}$. The latent heat of fusion ΔH_m is calculated either with the electrical resistivity variation (Fig. 8) or with the pyrometer response (Fig. 3). In both cases, its value is found to be $\Delta H_\mathrm{m} = (290 \pm 5)\,\mathrm{kJ}\cdot\mathrm{kg}^{-1}$ in very good agreement with previous data (average of several experiments) of (286 ± 3) [30] or $(295 \pm 15)\,\mathrm{kJ}\cdot\mathrm{kg}^{-1}$ [31].

On melting, the values for electrical resistivity without expansion correction are $\rho_{\mathrm{el0,s}} = 1.70\,\mu\Omega\cdot\mathrm{m}$ at the solidus and $\rho_{\mathrm{el0,l}} = 1.65\,\mu\Omega\cdot\mathrm{m}$ at the liquidus. It should be noted that such a decrease on melting has also been observed by Kaschnitz et al. [5]. Indeed, this corresponds to a behavior opposite to a very large majority of metals, as for the elements of the Ti-6Al-4V alloy such as Ti [20], Al [32], and V [33] or even another TiAl

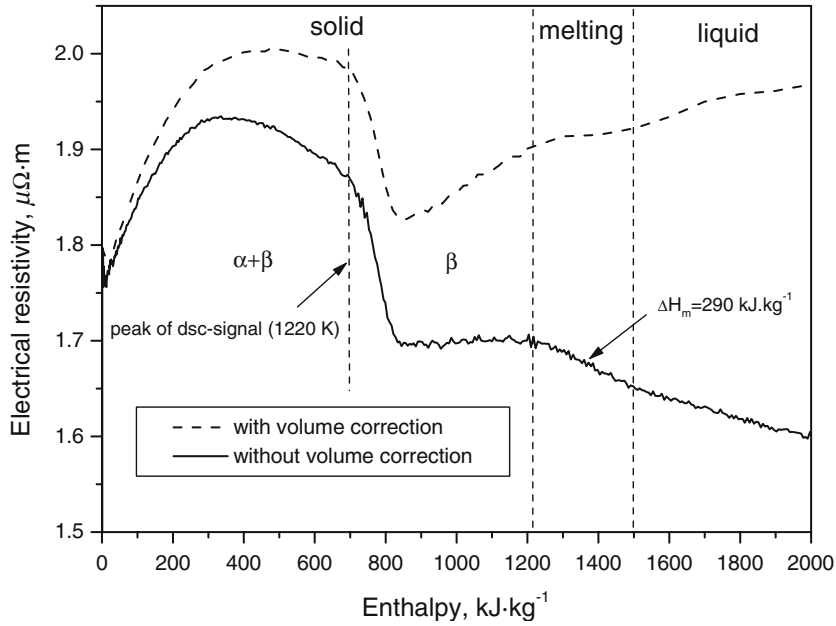

Fig. 8. Electrical resistivity versus enthalpy of solid and liquid Ti-6Al-4V with and without volume correction.

alloy [8]. Such a decrease of electrical resistivity disappears in both melting and the liquid phase by integrating the volume correction as shown in Fig. 8. Such results have already been observed on pure metals such as rhenium [34].

Corrected electrical resistivity values result in $\rho_{el0,s} = 1.90\,\mu\Omega \cdot \mathrm{m}$ at the solidus and $\rho_{el0,l} = 1.92\,\mu\Omega \cdot \mathrm{m}$ at the liquidus, meaning a slight increase during melting.

The specific volume variation has been also determined as a function of enthalpy as shown in Fig. 9. It was calculated according to Eq. (4) and radial expansion measurements obtained from Fig. 4. From these results, the volume expansion on melting ΔV_m is found to be $\Delta V_m = (3.9 \pm 0.3)\%$.

The normal spectral emissivity of liquid Ti-6Al-4V at $\lambda = 684.5\,\mathrm{nm}$ has been determined from laser polarimetry by using Eqs. (10) and (11), and is presented versus radiance temperature at 650 nm in Fig. 10. The emissivity results are the mean value of six individual and independent DOAP measurements. The normal spectral emissivity at 684.5 nm versus radiance temperature T_R can be described by the following linear least-squares fit:

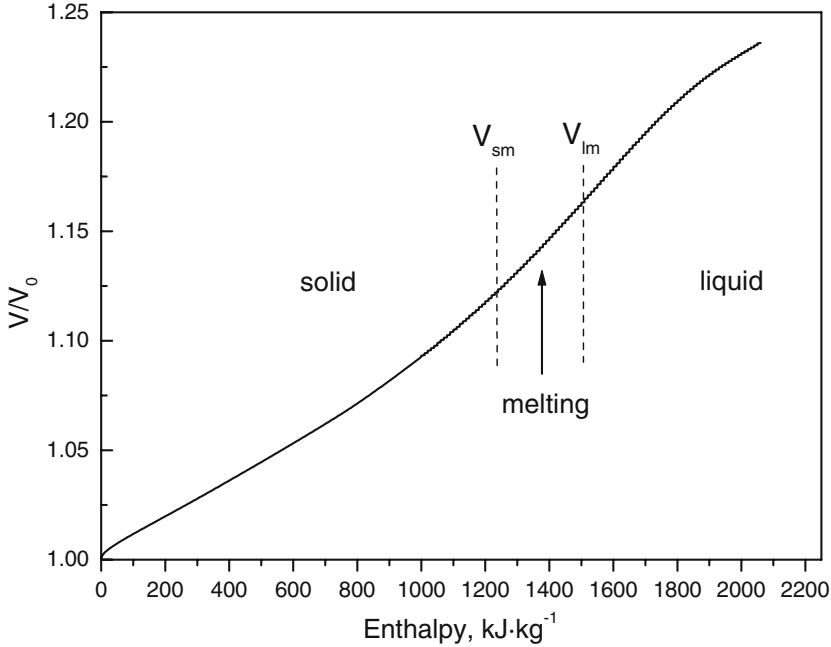

Fig. 9. Specific volume of solid and liquid Ti-6Al-4V versus enthalpy.

$$\varepsilon = 0.428 - 1.28 \times 10^{-5} T_{\mathrm{R}} \qquad 1788\,\mathrm{K} < T_{\mathrm{R}} < 2600\,\mathrm{K}. \tag{15}$$

Consequently, the linear least-squares fit to the liquid state of the normal spectral emissivity versus true temperature at 684.5 nm calculated from the emittance versus radiance temperature plot (Fig. 10) gives

$$\varepsilon = 0.425 - 1.05 \times 10^{-5}\, T \qquad T_{\mathrm{m}} < T < 2920\,\mathrm{K}. \tag{16}$$

The radiance temperature at the melting transition (which is assumed to be here the liquidus line as this alloy looks like a melting transition of pure metals rather than a solidus-liquidus transition as would be expected from an alloy) is obtained with $T_{\mathrm{R}} = 1788\,\mathrm{K}$. Furthermore, by using the extrapolated emissivity at the liquidus, a true temperature value of $T_{\mathrm{m}} = 1928\,\mathrm{K}$ is found in very good agreement with the material supplier (Goodfellow Cambridge Ltd.) data of 1873–1923 K for the melting temperature of Ti-6Al-4V.

One interesting issue with this alloy is the fact it takes an additional 200 K after the nominal melting temperature for emissivity to drop to a reproducible value in the liquid state. This behavior has also been found

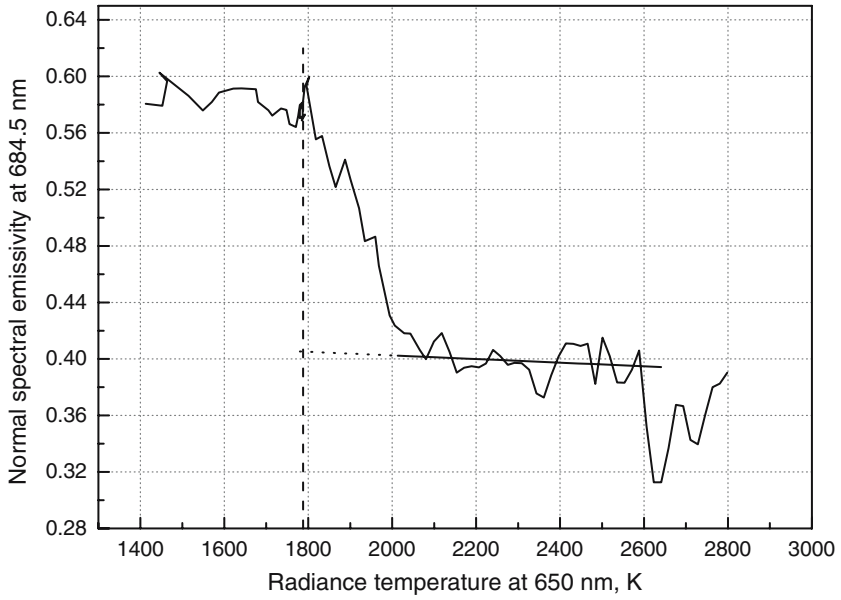

Fig. 10. Normal spectral emissivity at 684.5 nm versus radiance temperature at 650 nm. Straight line: linear least-squares fit to the liquid state; dotted line: linear least-squares values extrapolated to the liquidus temperature; vertical dashed line: liquidus temperature.

with zirconium and hafnium [26], both of which tend to have surface layers of oxides, nitrides, impurities, etc. As these surface layers can have melting temperatures that are significantly different from the melting temperature of the pure sample material, it might take some additional time (which equals a higher temperature during pulse-heating) for those surface layers to disappear (burn, get transparent, melt, etc.).

Such a phenomenon could also occur with Ti-6Al-4V as one of the components is aluminum, which has a much lower melting temperature (913 K) compared to the other two. Consequently, aluminum can be expected to be located in the outer regions of the wires, as the component with the lowest melting temperature is pushed to the surface. Furthermore, aluminum is known for its extremely fast growing oxide layer, which has completely different optical and physical properties. Then, such an aluminum oxide could be one of the main reasons for this 'delayed' drop in emissivity.

Moreover, since titanium is the main component within this alloy (about 90%), it is expected that some of the optical and physical properties are mainly influenced by titanium. This is especially true for the melting

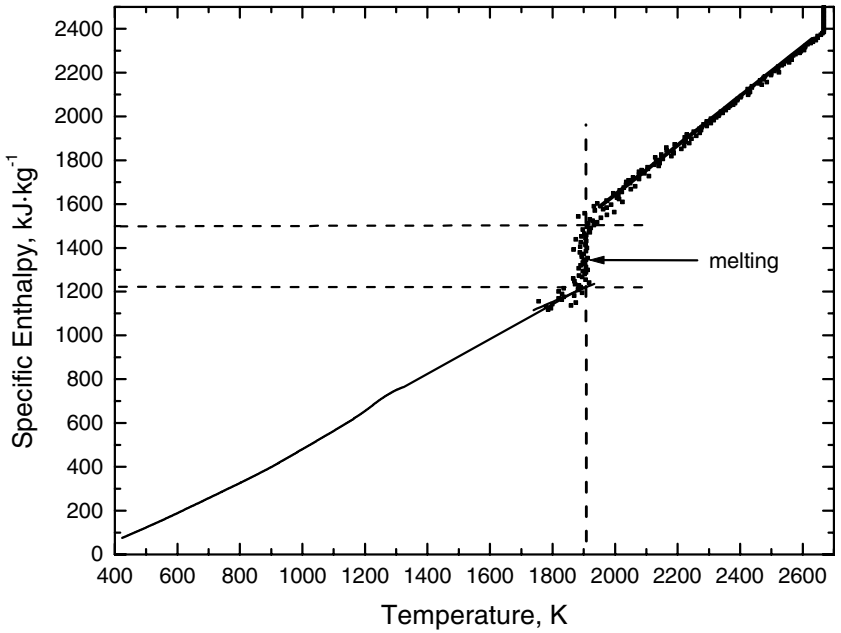

Fig. 11. Specific heat of solid (DSC) and liquid (pulse heating) Ti-6Al-4V.

temperature (which is very close to the melting temperature of pure titanium, $T_m = 1943\,K$) and also for the normal spectral emissivity value at the melting transition, ε in the liquid state, and also for the slight decreasing trend of emissivity throughout the liquid state.

Because the pyrometer threshold is around 1700 K, the low temperature range could not be measured from pulse experiments. Therefore, the DSC has been used for the $300 < T < 1600\,K$ range for solid Ti-6Al-4V, whereas temperature values were calculated from pulse heating experiments (see above) from 1700 K in the pre-melting range up to 2600 K in the liquid phase. By combining all of these data, the specific enthalpy is reported over the complete temperature range as presented in Fig. 11. The linear behavior of such a curve in the liquid phase is represented by

$$H(T) = -607.95 + 1.126T \qquad \text{for } T_m < T < 2600\,K \tag{17}$$

One can calculate the specific heat capacity c_p value of liquid Ti-6Al-4V from the slope of this curve (see Eq. (7)) which is found to be constant and equal to $1126\,J \cdot kg^{-1} \cdot K^{-1}$. This value is about 20% higher than $931\,J \cdot kg^{-1} \cdot K^{-1}$ obtained by Kaschnitz et al. [5]. Such a difference is not well explained and cannot be attributed to the material origin or

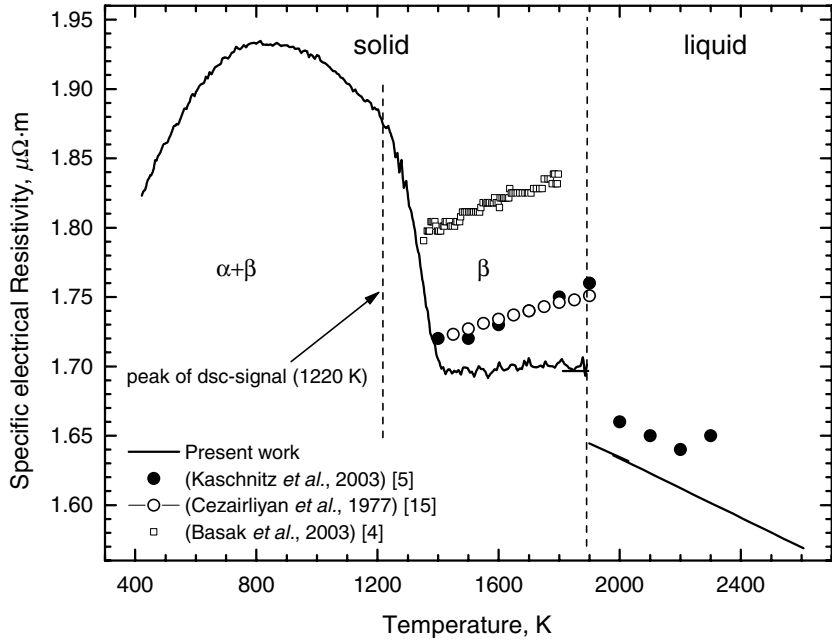

Fig. 12. Electrical resistivity versus temperature of solid and liquid Ti-6Al-4V and comparison with literature data (Basak et al., 2003 [4]; Cezairliyan et al., 1977 [15]; Kaschnitz et al., 2002 [5]).

manufacturing process (and associated thermomechanical treatments) since both electrical resistivity measurements of liquid Ti-6Al-4V show good agreement (see below). Moreover, our $1126\,J \cdot kg^{-1} \cdot K^{-1}$ value is very close to $1147\,J \cdot kg^{-1} \cdot K^{-1}$ obtained for another TiAl intermetallic alloy such as Ti-44Al-8Nb-1B [8].

Once the temperature is determined by combining DSC and pulse experiments, all the thermophysical properties can be reported as a function of temperature. Then, the electrical resistivity is reported in Fig. 12 versus temperature and is compared to available literature data in the melting region obtained by millisecond [4, 15] and microsecond [5] pulse-heating techniques. Agreement is good with Kaschnitz et al. and Cezairliyan et al., since our data are about $5\,\mu\Omega \cdot cm$ (i.e., 3%) lower than these literature values. However, a larger deviation ($\sim 10\ \mu\Omega \cdot cm$) is observed with Basak et al. results. As for c_p values (see Section 4), such a difference could be attributed to the origin and history of the material.

Moreover, our best linear fit of the electrical resistivity variation of liquid Ti-6Al-4V is as follows:

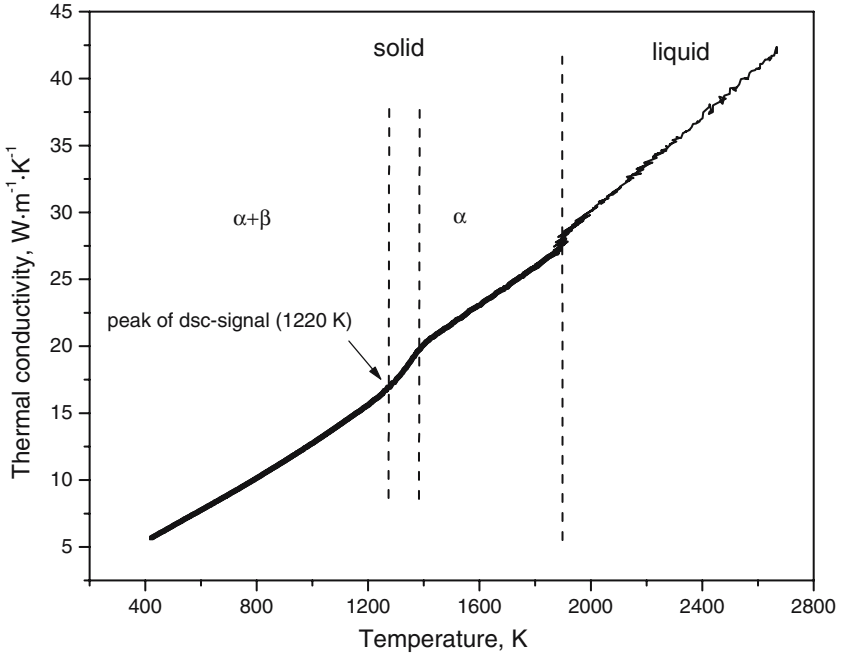

Fig. 13. Thermal conductivity of solid and liquid Ti-6Al-4V versus temperature.

$$\rho_{el}(T) = 1.85 - 1.07 \times 10^{-4} T \qquad \text{for } T_m < T < 2600\,\text{K}. \tag{18}$$

It should be noted that a negative slope of $d\rho_{el0}/dT$ of liquid Ti-6Al-4V was observed by Kaschnitz et al. [5] and also for Ti-44Al-8Nb-1B [8]. By incorporating the volume correction, it does indeed become positive as shown in Fig. 8.

The thermal conductivity has been determined by using the Wiedemann-Franz law (see Eq. (8)), and is presented in Fig. 13.

The linear fit for the β phase is found to be

$$\lambda_T = -0.32 + 1.46 \times 10^{-2}\, T \qquad 1400 < T < 1850\,\text{K} \tag{19}$$

and in the liquid phase:

$$\lambda_T = -6.66 + 1.83 \times 10^{-2}\, T \qquad 1950 < T < 2700\,\text{K} \tag{20}$$

where λ_T is in $\text{W} \cdot \text{m}^{-1} \cdot \text{K}^{-1}$ and T is in K.

The thermal diffusivity has also been calculated according Eq. (9) in the melting region (see Fig. 14), and leads to the following relationships according to the temperature ranges:

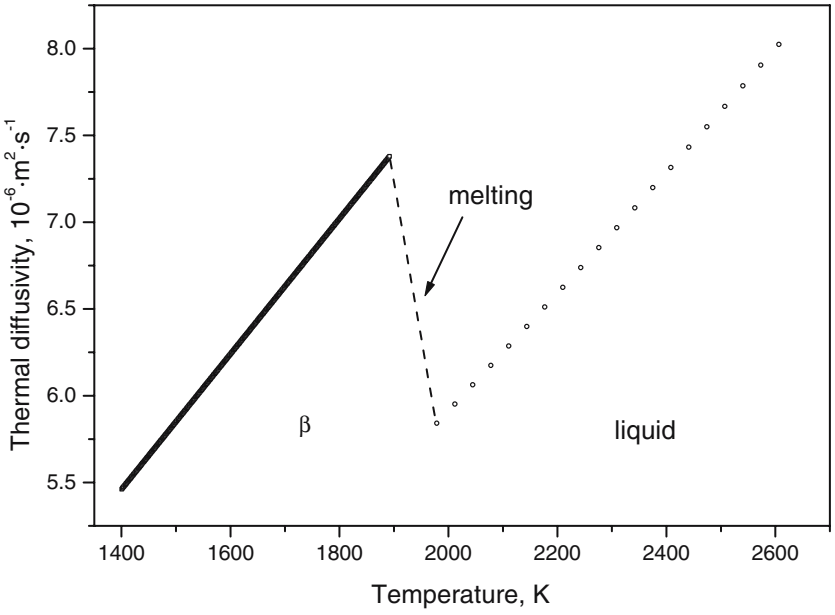

Fig. 14. Thermal diffusivity of solid and liquid Ti-6Al-4V versus temperature near the melting region.

$$a(T) = \left(-1.54 + 3.9 \times 10^{-2} T\right) 10^{-7} \qquad 1400 < T < 1850\,\mathrm{K} \tag{21}$$

and for liquid Ti-6Al-4V:

$$a(T) = \left(-1.54 + 3.9 \times 10^{-2} T\right) 10^{-7} \qquad 1950 < T < 2700\,\mathrm{K} \tag{22}$$

It should be reminded that the associated uncertainty of thermal conductivity and thermal diffusivity is $\pm 15\%$.

6. CONCLUSION

The thermophysical properties of solid and liquid industrial titanium alloy Ti-6Al-4V, namely electrical resistivity, specific heat capacity, volume expansion, spectral emissivity, thermal conductivity, and thermal diffusivity have been investigated up to 2700 K.

Transient techniques have demonstrated their unique capabilities of measuring thermophysical properties of materials under extreme experimental conditions. Such work confirms pulse heating experiments are also

well suited to studies on refractory alloys, stimulating a new investigation field, since the last several decades have been mainly focused on pure metals. However, one has to take care about the effect of the heating rate inducing a shift of solid phase transitions.

ACKNOWLEDGMENTS

The authors would like to thank L. Lalouat for his helpful contribution to bibliographic research, and L. Durut for her contribution to microstructure analysis. TU-Graz thanks the Austrian FWP for partly funding this work (Fund P15055).

REFERENCES

1. M. Boivineau and G. Pottlacher, submitted to International Journal of Materials Product and Technology. Special Issue: Challenges in Materials Properties Measurements.
2. G. R. Gathers, *Reports-on-Progress-in-Physics* **49**:341 (1986).
3. A. Cezairliyan, *High Temp. – High Press.* **11**:9 (1979).
4. D. Basak, R. A. Overfelt, and D. Wang, *Int. J. Thermophys.* **24**:1721 (2003).
5. E. Kaschnitz, P. Reiter, and J. L. McClure, *Int. J. Thermophys.* **23**:267 (2002).
6. D. Basak, W. J. Boetinger, D. Josell, S. R. Coriell, J. L. McClure, S. Krishnan, and A. Cezairliyan, *Acta Materialia* **47**:3147 (1999).
7. D. Basak, U. R. Kattner, J. L. McClure, D. Josell, and A. Cezairliyan, *Int. J. Thermophys.* **21**:913 (2000).
8. C. Cagran, B. Wilthan, G. Pottlacher, B. Roebuck, M. Wickins, and R. A. Harding, *Intermetallics* **11**:1327 (2003).
9. M. Kass, C. R. Brooks, D. Falcon, and D. Basak, *Intermetallics* **10**:951 (2002).
10. A. Seifter, G. Pottlacher, H. Jäger, G. Groboth, and E. Kashnitz, *Ber. Bunsenges. Phys. Chem.* **102**:1266 (1998).
11. V. N. Korobenko and A. I. Savvatimski, *J. Non-Cryst. Solids* **205–207**:678 (1996).
12. V. Didoukh, A. Seifter, G. Pottlacher, and H. Jager, *Int. J. Thermophys.* **19**:969 (1998).
13. H. J. Fecht and R. K. Wunderlich, *Proc. First Int. Symp. on Microgravity Research & Applications in Phys. Sci. & Biotechnol.*, Sorrento, Italy, 10–15 September 2000 (ESA SP-454, January, 2001), pp. 545–552.
14. A. Ludwig, *Int. J. Thermophys.* **23**:1131 (2002).
15. A. Cezairliyan, J. L. McClure, and R. Taylor, *J. Res. Nat. Bur. Stand.* **81A**:251 (1977).
16. C. R. Brooks, in *Heat treatment, Structures and Properties of Nonferrous Alloys* (American Society of Metals, Metals Park, Ohio, 1982), p. 361.
17. R. R. Boyer, G. Welsch, and E. W. Collings, in *Materials Properties Handbook – Titanium Alloys* (ASM International, 1994), p. 483.
18. G. Walsh, in *Materials Properties Handbook – Titanium Alloys* (ASM International, 1994).
19. H. Fujii and H. G. Suzuki, *Proc. Sixth World Conf. Titanium*, Cannes, France (June 1988), pp. 1489–1494.
20. A. Berthault, L. Arlès, and J. Matricon, *Int. J. Thermophys.* **7**:167 (1986).

21. M. Boivineau, *J. Nucl. Mat*. **297**:97 (2001).
22. R. Gallob, H. Jäger, and G. Pottlacher, *High Temp.-High Press*. **17**:207 (1985).
23. K. C. Mills, B. J. Monaghan, and B. J. Keene, *Int. Mat. Rev.* **41**:209 (1996).
24. A. Seifter, F. Sachsenhofer, S. Krishnan, and G. Pottlacher, *Int. J. Thermophys*. **22**:1537 (2001).
25. A. Seifter, F. Sachsenhofer, and G. Pottlacher, *Int. J. Thermophys*. **23**:1267 (2002).
26. C. Cagran, C. Brunner, A. Seifter, and G. Pottlacher, *High Temp.-High Press*. **34**:669 (2002).
27. EUML: Expression of the Uncertainty of Measurement in Calibration, EA-4/02, http://www.european accreditation.org/pdf/EA-4-02ny.pdf (1999).
28. B. Wilthan, C. Cagran, and G. Pottlacher, *Int. J. Thermophys*. **25**:1519 (2004).
29. A. Cezairliyan, J. L. McClure, and C. W. Beckett, *J. Res. Nat. Bur. Stand. (US)* **75A**:1 (1971).
30. J. L. McClure and A. Cezairliyan, *Int. J. Thermophys*. **13**:75 (1992).
31. R. F. Brooks, J. A. J. Robinson, L. A. Chapman, and M. J. Richardson, *High Temp.-High Press*. **35/36**:193 (2003/2004).
32. G. R. Gathers, *Int. J. Thermophys*. **4**:209 (1983).
33. G. R. Gathers, J. W. Shaner, R. S. Hixson, and D. A. Young, *High Temp.-High Press*. **11**:653 (1979).
34. Th. Thévenin, L. Arlès, M. Boivineau, and J. M. Vermeulen, *Int. J. Thermophys*. **14:**441 (1993).